PLANETARY SCIENCE

Measuring the melting curve of iron at super-Earth core conditions

Richard G. Kraus[1]*, Russell J. Hemley[2], Suzanne J. Ali[1], Jonathan L. Belof[1], Lorin X. Benedict[1], Joel Bernier[1], Dave Braun[1], R. E. Cohen[3], Gilbert W. Collins[4], Federica Coppari[1], Michael P. Desjarlais[5], Dayne Fratanduono[1], Sebastien Hamel[1], Andy Krygier[1], Amy Lazicki[1], James Mcnaney[1], Marius Millot[1], Philip C. Myint[1], Matthew G. Newman[6], James R. Rygg[4], Dane M. Sterbentz[1], Sarah T. Stewart[7], Lars Stixrude[8], Damian C. Swift[1], Chris Wehrenberg[1], Jon H. Eggert[1]

The discovery of more than 4500 extrasolar planets has created a need for modeling their interior structure and dynamics. Given the prominence of iron in planetary interiors, we require accurate and precise physical properties at extreme pressure and temperature. A first-order property of iron is its melting point, which is still debated for the conditions of Earth's interior. We used high-energy lasers at the National Ignition Facility and in situ x-ray diffraction to determine the melting point of iron up to 1000 gigapascals, three times the pressure of Earth's inner core. We used this melting curve to determine the length of dynamo action during core solidification to the hexagonal close-packed (hcp) structure. We find that terrestrial exoplanets with four to six times Earth's mass have the longest dynamos, which provide important shielding against cosmic radiation.

With the discovery of planets outside our Solar System, the search for life on other planetary bodies is one of the grand challenges of our time. This search among the diverse landscape of planets has driven the need for a deeper understanding of the formation and evolution of these extrasolar bodies. The sheer abundance of iron within rocky planet interiors motivates our need for a better understanding of the properties and response of iron at the extreme conditions deep in the cores of more massive Earth-like planets. Specifically, the iron melting curve is critical to understanding internal structure, thermal evolution, and the potential for dynamo-generated magnetospheres—a magnetosphere is believed to be an important component of habitable terrestrial planets, as it is on Earth (*1*, *2*).

Earth's magnetodynamo is generated in the convecting liquid outer core surrounding the solid inner core. Within the convecting liquid, as a parcel of iron descends toward the center of a planet, it is compressed at constant entropy, implying that it is compressed faster than heat can flow, but not so fast that viscous stresses dissipate substantial energy. The isentropic temperature profile in the liquid iron alloy in the outer core of Earth intersects the iron melting curve at ~330 GPa, forming the outer boundary of the solid inner core (*3*). The current highest-pressure melting curve data on pure iron reach only 290 GPa (*4*). The high pressure-temperature (*P-T*) phase relations also continue to be debated at these pressures despite the numerous studies that have been performed over the years (*5*–*9*). As a result of the sensitive interplay between the temperature profile and the melting transition defining the fate of iron-rich cores of rocky planets, a range of disparate predictions exist for magnetospheres of super-Earths. Some predict that only Earth-sized or smaller planets can have a liquid outer core, while anything larger will have a completely solid core (*10*). The opposite scenario has also been proposed, that is, that planets larger than Earth will have completely liquid cores (*11*). Another model suggests that planets larger than five Earth masses ($M_{\oplus}$) can have partially molten liquid outer cores (*12*). A core evolution model has also been proposed in which the iron isentrope is steeper, in the *P-T* plane, than the melting curve for bodies larger than a few Earth masses, causing iron crystallites to form at the outer radius of a liquid core and "snow" into the center of the planet, which the authors suggest will inhibit convection and a dynamo (*13*). This breadth of predicted phenomena is not unexpected given that the melting curve of iron is extrapolated by more than an order of magnitude in pressure for each of these models (*11*).

We experimentally determined the high-pressure melting curve and structural properties of pure iron up to 1000 GPa, or nearly four times greater pressure than any previous experiments. At the National Ignition Facility (NIF) of Lawrence Livermore National Laboratory (LLNL), we performed a series of seven experiments that emulate the conditions observed by a parcel of iron descending toward the center of a super-Earth core. As illustrated in Fig. 1, we tailored the laser power as a function of time for 16 NIF laser beams incident upon our sample package to first create a single steady shock wave in an iron sample, taking the iron to a state on the Hugoniot between 220 and 300 GPa and setting the entropy of the system. As the shock transits from the iron into a lithium fluoride (LiF) window, the iron decompresses isentropically to pressures between 120 and 160 GPa, ensuring a completely liquid iron sample for all but the lowest shock pressure experiment. Then we precisely increase the laser power to isentropically compress the sample to the desired peak pressure, up to 1000 GPa in ~10 ns, where the initial shock pressure and peak pressure in the sample are accurately determined from the measured interface velocity between the iron sample and LiF window (*14*). To document the atomic structure of the iron while it is at peak pressure, another 24 beams of the NIF laser illuminate a germanium or zirconium foil, producing a hot plasma. The plasma emits a ~1-ns burst of He-α radiation at 10.25 or 16.25 keV with a bandwidth of ~1%, allowing us to record an x-ray diffraction snapshot of the desired pressure state using image plates within the TARDIS diagnostic (*15*, *16*). A 400-μm-diameter pinhole of palladium or platinum attached to the sample package collimates the x-rays and casts a known diffraction pattern that we use to calibrate the location of the image plates in the TARDIS (*15*, *16*).

To constrain the melting curve, we performed sets of experiments at about the same peak pressure with different initial shock strengths, scanning entropy states that bound the melting curve. We present a summary of the in situ x-ray diffraction data (Fig. 1), where we observed pressure-driven solidification of iron from an initially liquid state into the hcp structure on the nanosecond time scale. With decreasing entropy at a given peak pressure, as within a cooling planet, the material state changes from liquid iron, as we evidenced by purely diffuse x-ray scattering, to a mixed state of hcp and liquid, and finally to solid hcp iron. At ~1000 GPa, corresponding to greater depths in a planet, we again observed the transition from liquid iron at high entropy states to solid hcp iron as the entropy is lowered, albeit at a higher entropy than at the 550 GPa peak pressure experiments.

The observation of pressure-driven solidification indicates that the melt curve is steeper than the isentrope. Our measured experimental bounds on the solidus and liquidus at two

[1]Lawrence Livermore National Laboratory, Livermore, CA 94550, USA. [2]Departments of Physics, Chemistry, and Earth and Environmental Sciences, University of Illinois at Chicago, Chicago, IL 60607, USA. [3]Earth and Planets Laboratory, Carnegie Institution for Science, Washington, DC 20015, USA. [4]Department of Mechanical Engineering, Department of Physics and Astronomy, and Laboratory for Laser Energetics, University of Rochester, Rochester, NY 14627, USA. [5]Sandia National Laboratories, Albuquerque, NM 87123, USA. [6]Division of Engineering and Applied Science, California Institute of Technology, Pasadena, CA 91125, USA. [7]Department of Earth and Planetary Sciences, University of California Davis, Davis, CA 95616, USA. [8]Department of Earth, Planetary, and Space Sciences, University of California Los Angeles, Los Angeles, CA 90095, USA.
*Corresponding author. Email: kraus4@llnl.gov

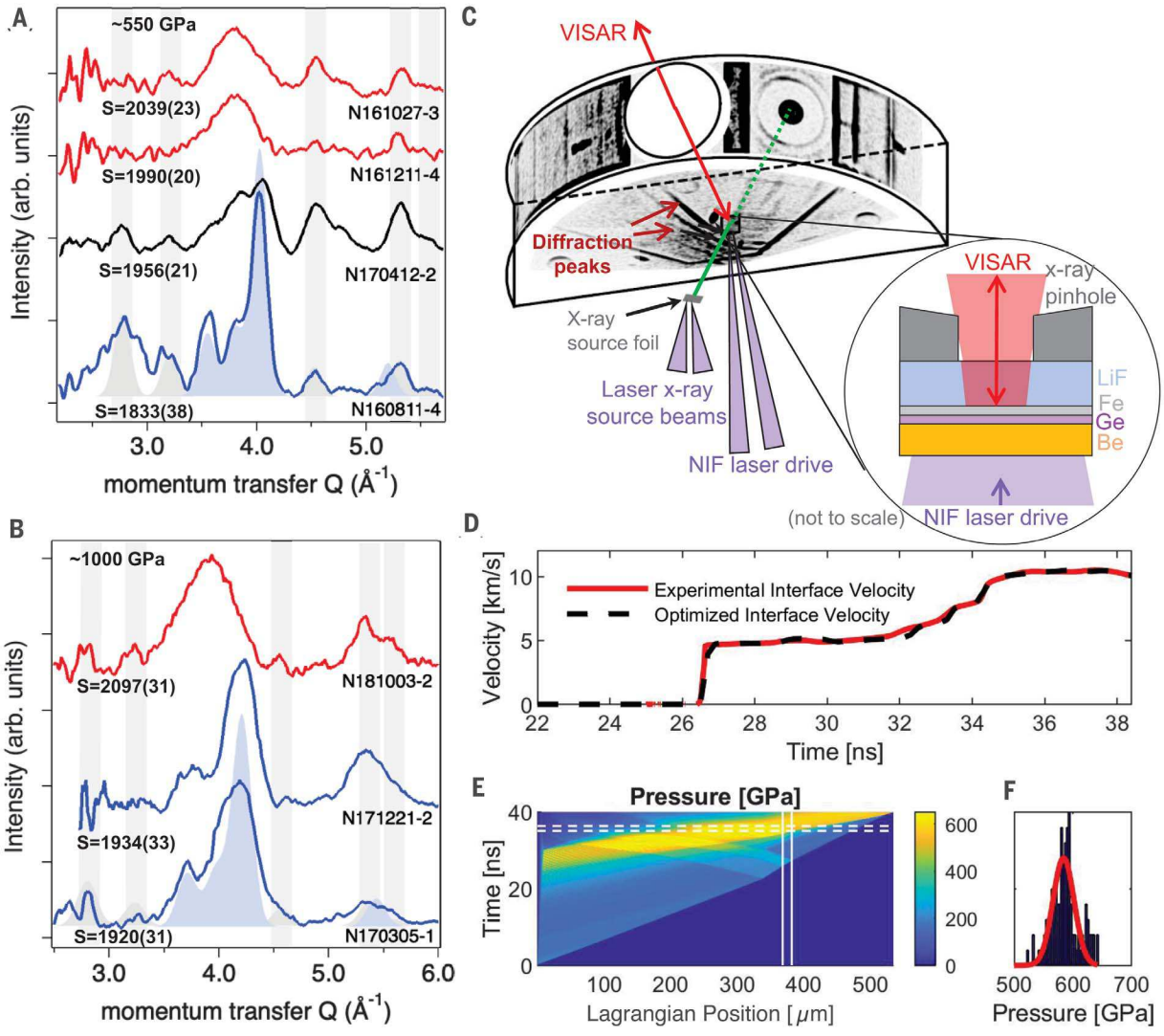

Fig. 1. Determining the phase assemblage of iron. (**A**) Diffraction lineouts for iron at ~550 GPa, with gray vertical bars marking the positions of diffraction peaks from the pinhole that are used for calibration. Red curves represent liquid iron; black, mixed-phase iron; and blue, hcp iron. The shaded blue area represents the ideal hcp pattern for the diagnostic resolution with a Ge backlighter. Also noted are the entropy states, *S*, in joules per kilogram per kelvin, and the shot numbers, *N*. (**B**) As in (A), but at a peak pressure of ~1000 GPa. (**C**) Schematic experimental configuration of the TARDIS diagnostic, with a zoomed-in view of the sample package that is attached to a collimating pinhole at the front of the TARDIS. (**D**) VISAR (velocity interferometer system for any reflector) data from N170412-2, which is used for direct impedance matching to determine the initial shock pressure and as input for a forward optimization (black dashed line). The forward optimization provides a pressure history throughout the sample package (**E**), from which one can infer the pressure history in the sample, defined by the vertical white bars, and (**F**), a pressure histogram of the iron during the x-ray exposure, denoted by the horizontal white dashed bars.

discrete peak pressures further constrain the melt curve to be steeper than the isentrope. These observations reaffirm the expected phenomena of bottom-up core solidification, where dynamo simulations show that the presence of bottom-up solidification will produce stronger magnetic fields than in the alternative case of top-down solidification (*17*). Furthermore, our observation of hcp iron along the melt curve combined with that of Turneaure *et al.* (*8*) refutes predictions of body-centered cubic stability in pure iron at core conditions (*18*, *19*), where it is noted that substantial alloying can affect phase stability and the mode of core solidification (*20*). Finally, the solidification into a mixed phase suggests that the nanosecond time scale of the experiments is not causing the transition to be substantially overdriven, where we might only expect to see a liquid or completely solidified system (*14*, *15*). This observation provides confidence in our measurement of the equilibrium melt curve.

Using available experimental data for the shock temperature and sound speed of iron in the liquid phase (*9*, *21*), we constrained the isochoric heat capacity, C_V = 4.2(1.0) kb per atom, and the Grüneisen parameter, γ = 1.51(5), along the Hugoniot from 6000 to 8000 K and 280 to 320 GPa. (*21*). The entropy on the Hugoniot is referenced to the high-temperature entropy of iron at 1 bar (*22*) via an isentrope intersecting the Hugoniot at 260 GPa and 5530 K (*15*). From analytic expressions for the entropy change along the Hugoniot (*23*), we obtained the entropy as a function of the shock pressure in each experiment (table S2). The solidus and liquidus are referenced to the pressures for incipient and complete melting

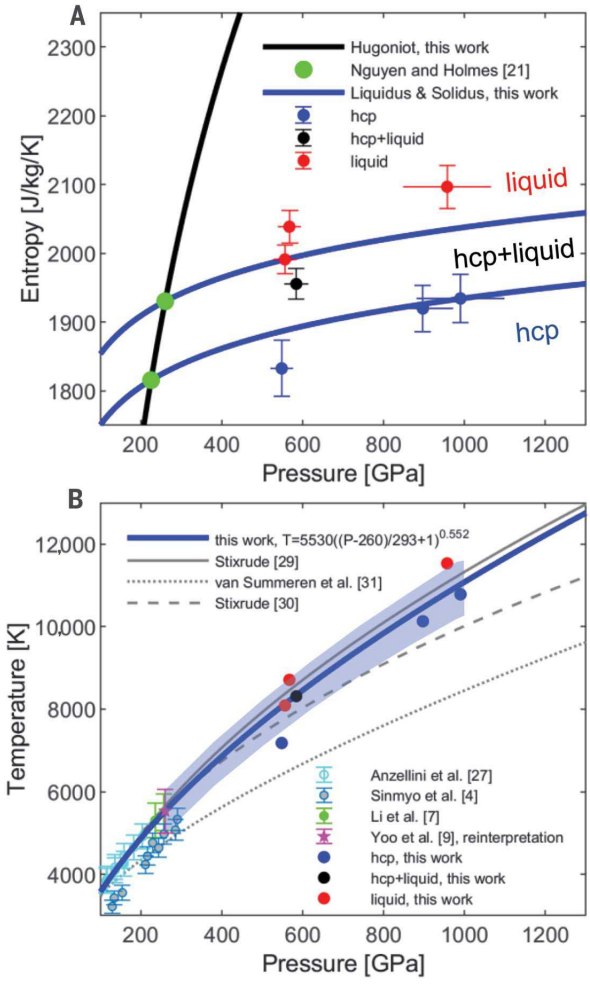

Fig. 2. The melting curve of iron. (**A**) Phase diagram of iron in the *P-S* plane. The phases we observed (hcp, hcp+liquid, and liquid) and the pressures for incipient and complete melting (*21*) were used to constrain power-law fits to the high-pressure melt curve (*15*). (**B**) Comparison of previous melting curve measurements on iron, all below 290 GPa, theoretical estimates, and our melting curve up to 1000 GPa. Transformation of measured melt curve from the *P-S* plane to *P-T* using experimentally constrained C_V and γ, with shaded 1σ uncertainties based on the uncertainty in the melt temperature at 260 GPa, *Cv*, γ, and our measured melt curve in the *P-S* plane. Also included are the phase measurements as a function of pressure and temperature, where individual 1σ temperature uncertainties are ~800 K.

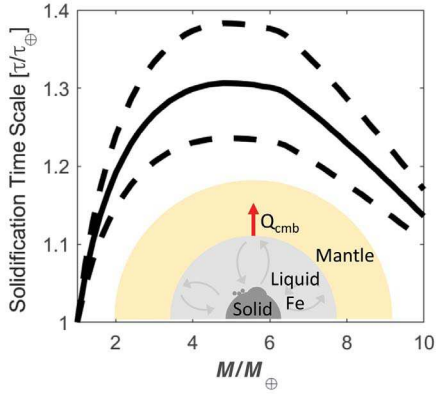

Fig. 3. Relative time scale for core solidification as a function of planetary mass. The time scale for solidification, τ, with dashed lines representing 1σ uncertainties, is based on the balance of heat flux out of the core, Q_{CMB} (*29*), with the reduction in entropy that is required to solidify the entire core (*15*). The time scale for solidification increases with planet mass, with a maximum in the 4 to 6 Earth mass ($M_\oplus$) regime. Our predicted time scale for solidification of Earth's core is 6.2(3.4) Gyr, where the lifetime of our star is ~9 to 10 Gyr and increases for lower-mass stars (*15*).

reported in (*21*) and then fit to the phase measurements obtained in this study, assuming a constant entropy of melting (Fig. 2).

Whereas the pressure-entropy (*P-S*) plane is the natural thermodynamic space for evaluating changes in phase along an isentrope, such as in volcanism or planetary impacts (*24*–*26*), the *P-T* plane is more common for comparing phase diagrams and assessing the accuracy of theoretical models. To convert our data, melt curve, and uncertainties into the *P-T* plane, we reevaluate the liquid phase–only shock temperature measurements of Yoo *et al.* (*9*). This eliminates complications associated with thermal conductivity and release paths in mixed phases. We then extrapolate the shock temperatures down to 260(3) GPa, the pressure of complete melting along the principal Hugoniot (*21*), and find the temperature on the melting curve of iron at 260(3) GPa to be 5530(530) K, which is in excellent agreement with the extrapolation of the melting curve of Anzellini *et al.* (*27*). From this reference point on the melting curve, our experimentally derived C_V and γ, and our measured curve in the *P-S* plane, we obtain the temperature along the melting curve from 260 to 1000 GPa through a two-step thermodynamic integration, with a Simon fit of the melting transition temperature $T_m = 5530\,[(P - 260)/293 + 1]^{0.552}$ (Fig. 2) (*15*).

Our direct measurements provide an experimentally constrained melting curve of iron to nearly four times greater pressure than any previous measurement. Although our data are focused on iron melting in super-Earth cores, our results also provide accurate determination of iron melting at the *P-T* conditions from the bottom of Earth's core through the inner core boundary (ICB), which has remained controversial because of the lack of direct measurements of melting through this regime. The differences in reported melting behavior of iron at core conditions have narrowed over the years, but the estimated T_m at the ICB at 330 GPa has still been based on extrapolation of data. Because our data provide information on the solidification of the cores of rocky planets well beyond the conditions of Earth's interior, we can interpolate to find the melting temperature of iron at the ICB, where we find T_m = 6230(540) K. This value is similar, within the uncertainties, to that extrapolated from lower-pressure melting data using thermodynamic constraints (*5*, *6*) and recent estimates (*4*, *7*, *8*). Comparing first-principles calculations, our results are consistent with, but somewhat shallower than, the density functional theory (DFT) fit (*28*) that Stixrude reported (*29*). Our melting curve is substantially steeper than that predicted by other DFT-based calculations (*30*) and the Lindemann-based melting curve used in magnetodynamo lifetime calculations (*31*).

Assuming Earth's core mass fraction and compressibility (*12*, *32*), we calculated pressure profiles within the mantles and cores of super-Earths. From this structure calculation and our measurement of the liquidus in the *P-S* plane, we directly determined how much the average entropy of the liquid iron core needs to drop to solidify from the center to the core-mantle boundary (CMB) as a function of planet size. Given that iron cores will likely start as completely liquid owing to the considerable entropy generation by giant impacts during the late stages of accretion (*15*, *33*, *34*) and assuming a CMB heat flux, Q_{CMB}, of $80(M/M_\oplus)$ mW m^{-2} (*29*), we estimate the time scale for solidification of super-Earth cores. We find that super-Earth cores will take up to 30% longer to solidify than Earth's core, where this model predicts Earth's core will solidify in 6.2(3.4) billion years (Gyr) (*15*) (Fig. 3), supporting estimates for a young inner core (*35*). Owing to competing effects of stored energy versus surface area, the cores of planets smaller than Earth will solidify quickly, with

the maximum time scale for solidification occurring in the 4- to 6-$M_\oplus$ size. Assuming the solidification time scale sets the time scale for dynamos, the results lead to the notable finding that super-Earths are likely to have a longer duration of magnetically shielded habitability than Earth.

REFERENCES AND NOTES

1. V. Dehant *et al*., *Space Sci. Rev.* **129**, 279–300 (2007).
2. L. Elkins-Tanton, *Eos* **94**, 149–150 (2013).
3. A. M. Dziewonski, D. L. Anderson, *Phys. Earth Planet. Inter.* **25**, 297–356 (1981).
4. R. Sinmyo, K. Hirose, Y. Ohishi, *Earth Planet. Sci. Lett.* **510**, 45–52 (2019).
5. O. L. Anderson, *Phys. Earth Planet. Inter.* **109**, 179–197 (1998).
6. R. J. Hemley, H. K. Mao, *Int. Geol. Rev.* **43**, 1–30 (2001).
7. J. Li *et al*., *Geophys. Res. Lett.* **47**, e2020GL087758 (2020).
8. S. J. Turneaure, S. M. Sharma, Y. M. Gupta, *Phys. Rev. Lett.* **125**, 215702 (2020).
9. C. S. Yoo, N. C. Holmes, M. Ross, D. J. Webb, C. Pike, *Phys. Rev. Lett.* **70**, 3931–3934 (1993).
10. D. Valencia, R. J. O'Connell, D. Sasselov, *Icarus* **181**, 545–554 (2006).
11. C. Sotin, O. Grasset, A. Mocquet, *Icarus* **191**, 337–351 (2007).
12. A. Boujibar, P. Driscoll, Y. Fei, *J. Geophys. Res. Planets* **125**, e2019JE006124 (2020).
13. E. Gaidos, C. P. Conrad, M. Manga, J. Hernlund, *Astrophys. J.* **718**, 596–609 (2010).
14. R. G. Kraus *et al*., *Phys. Rev. Lett.* **126**, 255701 (2021).
15. Materials and methods are available as supplementary materials.
16. J. R. Rygg *et al*., *Rev. Sci. Instrum.* **91**, 043902 (2020).
17. H. Cao *et al*., *Geophys. Res. Lett.* **41**, 4127–4134 (2014).
18. A. B. Belonoshko, R. Ahuja, B. Johansson, *Nature* **424**, 1032–1034 (2003).
19. W. Luo *et al*., *Proc. Natl. Acad. Sci. U.S.A.* **107**, 9962–9964 (2010).
20. F. Xu *et al*., *Earth Planet. Sci. Lett.* **563**, 116884 (2021).
21. J. H. Nguyen, N. C. Holmes, *Nature* **427**, 339–342 (2004).
22. M. W. Chase, *NIST-JANAF Thermochemical Tables*, Monograph No. 9 (American Institute of Physics, 1998).
23. S. Sugita, K. Kurosawa, T. Kadono, *AIP Conf. Proc.* **1426**, 895–898 (2012).
24. T. J. Ahrens, J. D. O'Keefe, *Moon* **4**, 214–249 (1972).
25. S. T. Stewart, A. Seifter, A. W. Obst, *Geophys. Res. Lett.* **35**, L23203 (2008).
26. R. G. Kraus *et al*., *J. Geophys. Res.* **117**, E09009 (2012).
27. S. Anzellini, A. Dewaele, M. Mezouar, P. Loubeyre, G. Morard, *Science* **340**, 464–466 (2013).
28. G. Morard, J. Bouchet, D. Valencia, S. Mazevet, F. Guyot, *High Energy Density Phys.* **7**, 141–144 (2011).
29. L. Stixrude, *Philos. Trans. R. Soc. London Ser. A* **372**, 20130076 (2014).
30. L. Stixrude, *Phys. Rev. Lett.* **108**, 055505 (2012).
31. J. van Summeren, E. Gaidos, C. P. Conrad, *J. Geophys. Res. Planets* **118**, 938–951 (2013).
32. R. F. Smith *et al*., *Nat. Astron.* **2**, 452–458 (2018).
33. P. J. Carter, S. J. Lock, S. T. Stewart, *J. Geophys. Res. Planets* **125**, e2019JE006042 (2020).
34. S. N. Raymond, E. Kokubo, A. Morbidelli, R. Morishima, K. J. Walsh, in *Protostars and Planets VI*, H. Beuther, R. S. Klessen, C. P. Dullemond, T. K. Henning, Eds. (Univ. of Arizona Press, 2014), pp. 595–618.
35. R. K. Bono, J. A. Tarduno, F. Nimmo, R. D. Cottrell, *Nat. Geosci.* **12**, 143–147 (2019).

ACKNOWLEDGMENTS

We thank B. Heidl, A. Nikroo, the NIF target fabrication team, and the NIF operations and management teams for their contributions to this research and the NIF Discovery Science Program for allocation of experimental time. **Funding:** This work was performed under the auspices of the US Department of Energy by Lawrence Livermore National Laboratory under contract DE-AC52-07NA27344. Sandia National Laboratories is a multi-mission laboratory managed and operated by National Technology and Engineering Solutions of Sandia, a wholly owned subsidiary of Honeywell International, for the US Department of Energy's National Nuclear Security Administration (DOE/NNSA) under contract DE-NA0003525. R.J.H. acknowledges support from DOE/NNSA (DE-NA0003975, CDAC). S.T.S. was supported by the Center for Matter under Extreme Conditions, funded by DOE/NNSA under award DE-NA0003842. G.W.C. and J.R.R. recognize support from NSF Physics Frontier Center award PHY-2020249. R.E.C. gratefully acknowledges the Gauss Centre for Supercomputing e.V. (www.gauss-centre.eu) for funding this project by providing computing time on the GCS Supercomputer SuperMUC-NG at Leibniz Supercomputing Centre (LRZ, www.lrz.de) and support from NSF grant EAR-1901813 and the Carnegie Institution for Science. **Author contributions:** Conceptualization: R.G.K., R.J.H., R.E.C., G.W.C., S.T.S., L.S., and J.H.E. Experiment design: R.G.K., D.B., D.F., A.L., J.R.R., D.C.S., and J.H.E. Data acquisition: R.G.K., J.B., F.C., D.F., A.L., J.M., J.R.R., C.W., and J.H.E. Data analysis: R.G.K., S.J.A., F.C., D.F., A.K., A.L., M.M., M.G.N., J.R.R., and J.H.E. Data interpretation: R.G.K., R.J.H., J.L.B., L.X.B., M.P.D., S.H., A.L., P.C.M., D.M.S., J.H.E., S.T.S., and L.S. Writing – original draft: R.G.K. Writing – review and editing: All authors. **Competing interests:** The authors declare that they have no competing interests. **Data and materials availability:** All data are available in the main text or the supplementary materials.

SUPPLEMENTARY MATERIALS

science.org/doi/10.1126/science.abm1472
Materials and Methods
Supplementary Text
Figs. S1 to S39
Tables S1 and S2
References (*36*–*76*)

28 August 2021; accepted 6 December 2021
10.1126/science.abm1472

Measuring the melting curve of iron at super-Earth core conditions

Richard G. KrausRussell J. HemleySuzanne J. AliJonathan L. BelofLorin X. BenedictJoel BernierDave BraunR. E. CohenGilbert W. CollinsFederica CoppariMichael P. DesjarlaisDayne FratanduonoSebastien HamelAndy KrygierAmy LazickiJames McnaneyMarius MillotPhilip C. MyintMatthew G. NewmanJames R. RyggDane M. SterbentzSarah T. StewartLars StixrudeDamian C. SwiftChris WehrenbergJon H. Eggert

Science, 375 (6577),

Terapascal iron-melting temperature

The pressure and temperature conditions at which iron melts are important for terrestrial planets because they determine the size of the liquid metal core, an important factor for understanding the potential for generating a radiation-shielding magnetic field. Kraus *et al*. used laser-driven shock to determine the iron-melt curve up to a pressure of 1000 gigapascals (see the Perspective by Zhang and Lin). This value is about three times that of the Earth's inner core boundary. The authors found that the liquid metal core lasted the longest for Earth-like planets four to six times larger in mass than the Earth. —BG